CrossMark

RESEARCH PAPER

Potential of two-line atomic fluorescence for temperature imaging in turbulent indium-oxide-producing flames

Bettina Münsterjohann · Franz J. T. Huber · Tobias C. Klima ·
Sandra Holfelder · Sascha R. Engel · Joseph D. Miller ·
Terrence R. Meyer · Stefan Will

Abstract The applicability of two-line atomic fluorescence (TLAF) for temperature imaging in an indium-based flame spray pyrolysis (FSP) process is demonstrated using a single tunable optical parametric oscillator (OPO) to generate the required excitation wavelengths consecutively. Single-shot images of the detected fluorescence signals demonstrate that the signal levels in the flame are suitable for evaluation of temperature and verify the capability and potential of the measurement technique directly during particle formation without additional indium seeding. Qualitative averaged two-dimensional temperature distributions in the FSP flame are presented, showing the influence of varying sheath gas flow rates on the resulting temperature distribution. With the addition of a second OPO and detection system, the two fluorescence signals acquired consecutively in this work could be obtained simultaneously and enable spatio-temporally resolved single-shot temperature measurements in flame synthesis processes of indium-containing nanoparticles.

Keywords Flame spray pyrolysis · Indium(III)-oxide nanoparticles · Two-line atomic fluorescence · Temperature measurement

B. Münsterjohann · F. J. T. Huber · T. C. Klima ·
S. Holfelder · S. R. Engel · S. Will (✉)
Lehrstuhl für Technische Thermodynamik (LTT),
Friedrich-Alexander Universität Erlangen-Nürnberg
(FAU), Erlangen, Germany
e-mail: stefan.will@fau.de

B. Münsterjohann · F. J. T. Huber · T. C. Klima ·
S. Holfelder · S. R. Engel · T. R. Meyer · S. Will
Erlangen Graduate School in Advanced Optical
Technologies (SAOT), Friedrich-Alexander-Universität
Erlangen-Nürnberg (FAU), Erlangen, Germany

B. Münsterjohann · F. J. T. Huber · S. Holfelder ·
S. R. Engel · S. Will
Cluster of Excellence Engineering of Advanced Materials
(EAM), Friedrich-Alexander-Universität Erlangen-
Nürnberg (FAU), Erlangen, Germany

J. D. Miller
Air Force Research Laboratory, Aerospace Systems
Directorate, Wright-Patterson AFB, OH, USA

T. R. Meyer
School of Mechanical Engineering, Purdue University,
West Lafayette, IN, USA

Introduction

Flame spray pyrolysis (FSP) processes are used to produce tailored nanoparticles on a commercial scale (Kammler et al. 2001; Teoh et al. 2010). Among other gas-phase techniques, FSP is one of the most versatile, cost-effective, scalable, and manageable processes (Camenzind et al. 2005; Strobel and Pratsinis 2007). Therefore, it is widely used in research and in industry for the synthesis of a broad spectrum of complex and functional nanomaterials including titanium dioxide (TiO_2), silica (SiO_2), zinc oxide (ZnO), indium tin oxide (ITO) or indium(III)-oxide (In_2O_3) (Mädler et al. 2002; Jang et al. 2006). Indium(III)-oxide is a n-type semiconductor with the unusual combination of high transparency in the visible region and high electrical conductivity (Gopchandran et al. 1997). These properties make indium oxide nanoparticles interesting for a number of applications such as electro-optic modulators, low-emissivity windows, solar cells, flat-panel displays, and electrochromic mirrors (Gopchandran et al. 1997; Murali et al. 2001).

One of the most important factors that influence particle size, morphology, and crystallinity is the temperature distribution during nanoparticle formation within the flame. Higher flame temperatures lead to faster precursor decomposition and an increase in supersaturation, which reduces the primary particle size at identical residence times (Kammler et al. 2001). Therefore, detailed information concerning the gas-phase temperature distribution in the flame is of specific interest. Classical invasive measurement techniques such as thermocouple measurements change the local process conditions and product properties significantly, whereas laser-based imaging techniques provide temperature information without perturbing the investigated system (Kronemayer et al. 2007). The challenges in applying optical measurement techniques in the FSP process are caused by scattering of optical wavelengths, high gas temperatures, large temperature gradients, and the unsteady character of the sprays (Engel et al. 2012).

Non-intrusive temperature measurements in particle-laden flames have been demonstrated using Fourier-transform infrared (FTIR) emission/transmission (E/T) spectroscopy (Kammler et al. 2003; Arabi-Katbi et al. 2001), which compares the normalized radiance with the best fit of the blackbody Planck function. In contrast to FTIR E/T spectroscopy, the coherent anti-Stokes Raman scattering (CARS) technique (Engel et al. 2012) provides detailed temporal and spatial temperature information in sooting and particle-laden flames. This technique, however, is normally limited to pointwise temperature measurements. While recent advances in CARS spectroscopy have made planar measurements possible (Bohlin and Kliewer 2013), the spatial extent of CARS measurements is insufficient for thermometry over the spatial scales of the flame spray pyrolysis process. Additionally, the technique suffers from high experimental effort. Vibrational and rotational Raman techniques have been used for temperature measurements in sooting and particle-laden flames as well (Stricker 2002; Liu et al. 2010), but are often restricted to line measurements and the accuracy is limited since knowledge of the collisional cross-sections is required for all involved species (Hartlieb et al. 2000). Two-dimensional temperature imaging can be obtained by filtered Rayleigh scattering (Müller et al. 2014), which requires knowledge on the local gas composition, or laser-induced fluorescence (LIF) (Daily 1997) using either seeded or naturally occurring molecular species in the combustion process. One of the most commonly used native molecules for LIF is the OH radical (Kohse-Hönghaus 1994), which, however, exhibits low concentrations in fuel-rich and sooting flames due to the low prevailing temperatures and low levels of oxidizing species present (Haudiquert et al. 1997). Bessler et al. (2000) showed temperature distribution in rich flames using two-line LIF by seeding nitric oxide (NO), and Kronemayer et al. (2007) measured two-dimensional gas-temperature fields by multi-line NO-LIF in a low-pressure flat flame during nanoparticle synthesis. In their approach, however, scanning of the wavelengths was required, limiting the temporal resolution. Since NO is a chemically active combustion species, the seeded NO is reduced by a combination of reburn, chemistry, and dilution (Nygren et al. 2001). For this reason, large amounts of NO are necessary to achieve the signal-to-noise ratios required for LIF thermometry. Another opportunity is the usage of atomic species as tracers, which benefits from the simpler spectroscopic features of an atom (Daily 1997). For instance, seeded gallium atoms have been used in a fuel-rich flame for thermally assisted fluorescence (THAF) measurements (Joklik et al. 1991). This technique requires again the knowledge of collisional cross-sections for

all involved species, which is difficult to assess in highly sooting or turbulent flames.

In this context, two-line atomic fluorescence (TLAF) with indium as tracer species is an attractive alternative, since this technique is not affected by molecular collisions and quenching effects (Daily 1997). Indium is a preferred species for thermometry due to its high sensitivity over a wide temperature range (800 - 2800 K) (Nygren et al. 2001). In the literature, this technique has been applied for temperature measurements in sooting flames and combustion environments using an aqueous solution of indium(III)-chloride ($InCl_3$) for seeding (Nygren et al. 2001; Medwell et al. 2009). Here, the technique is extended to application in an indium-based FSP process during particle formation of indium(III)-oxide (In_2O_3). In comparison to conventional TLAF, no additional indium seeding is needed. In this proof-of-concept study, a single optical parametric oscillator (OPO) is used to generate both excitation wavelengths consecutively, with the goal of evaluating signal levels that would allow two-dimensional temperature measurements. This setup of course does not allow for simultaneous measurements of the two fluorescence signals. However, the potential of the technique for temporally and spatially resolved single-shot temperature measurements during the FSP process is successfully shown.

Experimental approach

Burner system

Figure 1 shows the schematic of the FSP process using a burner system (Tethis S.p.A., Nano Powder Nozzle) with an annular design (diameter $\varnothing = 80$ mm, height $h = 50$ mm). The precursor indium(III)-acetyl-acetonate ($In(acac)_3$) dissolved in the organic solvent ethanol is injected through a capillary tube (inner diameter: 0.41 mm and outer diameter: 0.72 mm), placed in the center of the burner (a). Around this capillary tube, the dispersion gas oxygen is injected through a nozzle (b) in a coflow configuration. The tube ends 0.5 mm above the nozzle exit. This leads to a rapid atomization and prevents liquid from penetrating the gas line (Engel et al. 2012). The pressure drop of the dispersion gas is measured by a pressure transducer and can be adjusted manually with an
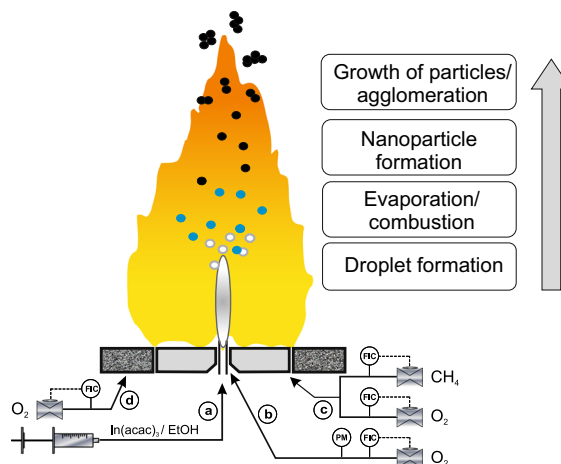

Fig. 1 Schematic of the FSP process including flow controllers (FlC) and pressure measurement (PM). **a** Precursor indium(III)-acetyl-acetonate ($In(acac)_3$) dissolved in the organic solvent ethanol, **b** dispersion gas (O_2), **c** support flame gases (O_2 + CH_4), **d** sheath gas (O_2)

external adjustment thread. The slit of the annular outlet of the premixed methane and oxygen support flame (c) is concentrically arranged around the injection tube at a radial distance of 5 mm. The support flame is used to ignite and sustain the spray combustion (Strobel and Pratsinis 2007). Around the support flame, an oxygen sheath gas flows through a sintered stainless steel ring plate with a pore size of approximately 50 μm to stabilize and shield the spray flame (d). The volume flow rates of oxygen and methane are regulated separately for the support flame, the dispersion, and the sheath gas using mass flow controllers. The investigated flame conditions are given in Table 1. The precursor solution, composed of 0.0128 mol/l or 5.3 mg/ml $In(acac)_3$ (ABCR, purity 98 %) dissolved in the organic solvent ethanol (Merck, purity > 99.8 %), is injected with a flow rate of 5 ml min^{-1} generated by a syringe pump (AITECS SEP-10S Plus). The precursor spray of the organic solution is ignited and sustained by the support flame. For the measurements presented here, the equivalence ratio of the support flame, not considering the precursor, dispersion gas and sheath gas volume flow, was set to $\Phi = 1.0$. Evaporation and combustion of the precursor/ethanol droplets result in a local supersaturation of In_2O_3. Thereupon primary particles are formed by nucleation. Furthermore, growth, agglomeration, and sintering of particles take place in higher regions of the flame (Engel et al. 2012). The different flame zones

Table 1 Flame conditions for sheath gas study

Precursor	In(acac)$_3$ / EtOH
$\dot{V}_{pre}$	5.0 mlmin^{-1}
c_{pre}	0.0128 mol l^{-1}
$\dot{V}_{O_2,SG}$	4.0 / 10.0 / 16.0 lmin^{-1}
$\dot{V}_{O_2,DG}$	5.0 lmin^{-1}
$\dot{V}_{O_2,SF}$	3.0 lmin^{-1}
$\dot{V}_{CH_4,SF}$	1.5 lmin^{-1}
Δp_{DG}	1.5 bar

pre precursor, *SG* sheath gas, *DG* dispersion gas, *SF* support flame

for particle formation are illustrated in Fig. 1 and are described in detail by Kilian et al. (2013).

Measurement technique and optical setup

The applied measurement technique TLAF is based on the optical excitation of two transitional states of indium atoms in the flame at 410.18 and 451.13 nm and the subsequent detection of the spectrally shifted fluorescence signals (Medwell et al. 2009). The population distribution of the temperature sensitive states is probed by measuring the Stokes and anti-Stokes direct-line fluorescence from a common upper state (Hult et al. 2005). Further details about the theory of TLAF are given in Daily (1997) and Medwell et al. (2009) and references therein. The temperature can be evaluated from the ratio of the corresponding fluorescence signals by combining the rate equations with the Boltzmann population equation. For the present linear excitation regime, the temperature T is given by Dec and Keller (1986):

$$T = \frac{\Delta E_{21}/k_B}{\ln\left(\frac{F_{32}}{I_{13}}\right) - \ln\left(\frac{F_{31}}{I_{23}}\right) + 4\ln\left(\frac{\lambda_{32}}{\lambda_{31}}\right) + C_t}. \quad (1)$$

Here, ΔE_{21} is the energy separation between the ground state 1 ($5^2P_{1/2}$) and level 2 ($5^2P_{3/2}$), k_B is the Boltzmann constant, F_{32} is the measured fluorescence signal between levels 3 ($6^2S_{1/2}$) and 2 ($5^2P_{3/2}$) (Stokes), F_{31} is the measured fluorescence signal between levels 3 ($6^2S_{1/2}$) and 1 ($5^2P_{1/2}$) (anti-Stokes), I is the laser spectral irradiance, λ is the wavelength, and C_t is a non-dimensional calibration constant

dependent on experimental factors (e.g., collection efficiency of the detectors, transmission characteristics of filters (Hult et al. 2005)).

In the present work, the required excitation wavelengths for TLAF are generated by a custom-built OPO (Miller et al. 2012) pumped by a multi-mode, Q-switched, frequency-tripled Nd:YAG laser with pulse energies up to 325 mJ/pulse at 355 nm and a repetition rate of 30 Hz (Quanta Ray PRO-250-30, Spectra Physics). OPO devices have been used extensively for high-resolution spectroscopy because of their wide tunability and high-speed operation owing to the use of solid-state crystals for frequency conversion (Miller et al. 2011). The pump pulse energy was varied from 1 to 35 mJ by adjusting the Q-switch time delay, and the beam diameter was reduced to 3 mm by a circular aperture. The OPO cavity is arranged in a ring configuration as shown in Fig. 2 and is described in previous work (Miller et al. 2012). The ring configuration permits co-directional pumping of the non-linear crystals and therefore simplifies the introduction of signal-resonant injection-seeded light into the cavity when linewidth narrowing is employed. Pump light enters and exits the cavity via two intracavity mirrors designed for high reflectance at 355 nm and antireflection (AR) coated from 400 to 450 nm, the signal wavelengths. The OPO consists of two BBO (β-barium-borate) crystals (7 × 7 × 15 mm, United Crystals) cut at 25° for Type I phase matching and oriented to compensate for pump–signal walkoff due to differences in the index of refraction in the ordinary and extraordinary axes. In this work, the cavity comprises two high-reflectivity mirrors (99 % reflectivity from 375 to 460 nm) and one output coupler (40 % nominal reflectivity from 390 to 460 nm). A maximum conversion efficiency of 5.1 % at 410.18 nm and 12 % at 451.13 nm was obtained by varying the pump pulse energy from 1 to 35 mJ and recording the signal pulse energy. The corresponding bandwidth (FWHM) is 2.08 cm^{-1} at 410.18 nm and 1.47 cm^{-1} at 451.13 nm. Broadband output was utilized in this work to excite all hyperfine components within the $5^2P_{1/2}$, $F = 4,5 \rightarrow 6^2S_{1/2}$, $F' = 4,5$ transition at 410.13 nm (maximum separation <0.7 cm^{-1}), and $5^2P_{3/2}$, $F = 3,4,5,6 \rightarrow 6^2S_{1/2}$, $F' = 4,5$ transition at 451.13 nm (maximum separation <0.4 cm^{-1}) (Rasbach et al. 2004). Under these conditions, a linear relationship between excitation
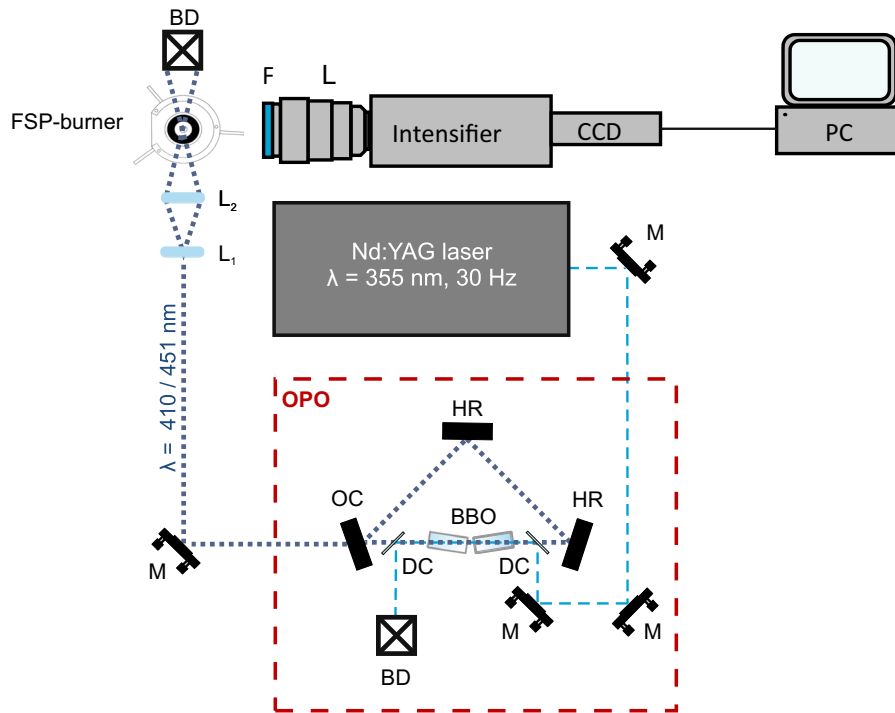
Fig. 2 Optical setup for TLAF measurements. *OPO* optical parametric oscillator, *HR* high reflector, *OC* output coupler (40 % reflective), *DC* dichroic mirror, *BBO* β-barium-borate crystal, *BD* beam dump, *L* lens, *M* mirror, *F* filter, *CCD* charge-coupler device

energy and signal intensity was verified for constant indium concentration at both transitions.

In order to obtain two-dimensional temperature information in the flame, the laser beam is formed to a diverging light sheet. The employed lens system is sketched in Fig. 2. It consists of two cylindrical lenses: the first lens with $f_1 = 40$ mm expands the laser beam in the vertical direction, and the second lens with $f_2 = 156$ mm reduces the light sheet thickness in the measurement volume to a minimum of about 2 mm. The limiting aperture for the light sheet is the second cylindrical lens with a height of 70 mm. The fluorescence signals are recorded consecutively after realigning the OPO by a camera system comprising a high-sensitivity digital camera (E-lite, LaVision) with a 50 mm camera lens (Nikon Nikkor, 1:1.2), an intensifier (IRO = intensified relay optics, LaVision) and a controller. Two different bandpass filters are used for the detection of the fluorescence signals to suppress the detection of elastically scattered light of the excitation wavelength and interference from other laser-excited species. First, a laser clean-up filter (ZET 405/20), transmitting light at

405 nm with a bandwidth of 20 nm, was used for the excitation wavelength 410.18 nm, and second, a brightline filter (HC 448/20), transmitting light at 448 nm with a bandwidth of 20 nm, was applied for the laser wavelength 451.13 nm.

Data evaluation and results

In Fig. 3, two collected single-shot images are exemplified for 410.18 and 451.13 nm laser excitation, with fluences H of about 4 J/m² at 410.18 nm and 3 J/m² at 451.13 nm. While the OPO could be operated at either wavelength, instantaneous measurement of the signal ratio would require a second OPO, which was not available for this proof-of-concept study. For each single-shot image of a certain excitation wavelength, a signal-to-noise ratio (SNR) in the region of interest (ROI) can be determined. Here, the ROI was deliberately set to a flame region (centered at 40 mm HAB, 100×100 pixels) where medium fluorescence intensities occur, in order to get a realistic SNR value. By averaging SNRs from single-shot images, a mean SNR

Fig. 3 Single-shot images of the fluorescence signal with an excitation wavelength of **a** 410.18 nm and **b** 451.13 nm and detection wavelength of **a** 451 nm and **b** 410 nm, respectively. ROI for SNR calculation (*white square*)
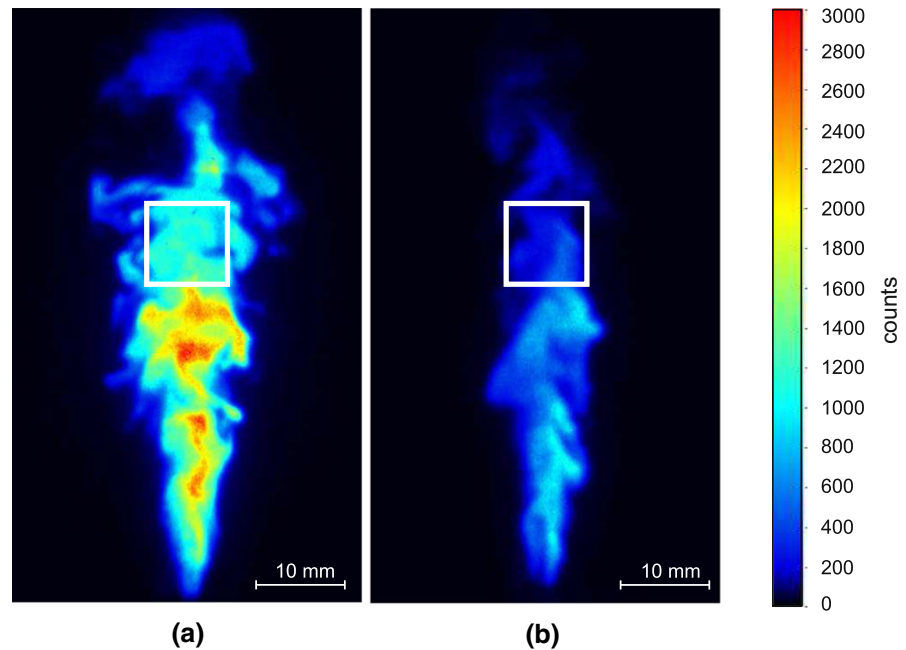

of 42 and 33 for 410.18 and 451.13 nm can be obtained, respectively. By application of error propagation, these values result in a mean temperature error in the ROI of 11 K, showing that despite the relatively low indium concentration of 0.0128 mol/l in the precursor solution, the fluorescence signal is sufficient to reveal the instantaneous turbulent flow structure and to allow for a calculation of signal ratios on a shot-to-shot basis for temperature imaging.

As excitation and detection at the two different wavelengths were not carried out simultaneously, only averaged fluorescence data over 200 images are considered in the following temperature calculation. At this point, the calibration constant C_t has to be determined by a reference temperature measurement. CARS is a standard and very precise technique for temperature measurement and thus chosen for calibration of the TLAF setup in this work. The constant C_t is based on temperatures from CARS measurements in the FSP process measured by Engel et al. (2012) during silica production. As the same flame conditions (volume flow rates of gases and precursor) except for precursor composition and concentration are used (HMDSO was exchanged for In(acac)$_3$), the CARS-temperature results are still applicable because the indium concentration in the precursor has only a

small influence on the temperature. From Engel et al. (2012), we obtained ten temperatures in five radial positions at two different heights above the burner surface (HAB). The CARS temperature at the center position in 25 mm HAB was used for calibration of TLAF as the fluorescence signal in this position was the most intense. From processing the respective fluorescence signals from the two excitation/detection schemes, a direct determination of the local temperature within the resolution of a pixel (0.09 × 0.09 mm^2) is possible (see Fig. 4), obtaining a two-dimensional map of local temperature. Due to extinction effects, mainly caused by absorption, the excitation and fluorescence signals may be affected. For this reason, a correction of these effects is performed. For each detection wavelength, the fluorescence signal F is normalized by the corresponding laser fluence H. To determine the local fluence, first the spatial distribution of the local fluence has to be known. To this end, the spatial fluence profile of the laser light sheet, irradiating a Lambertian surface (white paper) under an angle of 45 ° relative to the beam and detection plane, is recorded by the intensified CCD-camera. To obtain a fluence correction image, the background corrected spatial fluence profile is integrated along the thickness of the light sheet as the fluorescence signal is integrated along this

Fig. 4 Influence of different sheath gas flow rates on the distribution of averaged temperatures in the flame, **a** $\dot{V}_{O_2,SG} = 4$ l/min; **b** $\dot{V}_{O_2,SG} = 10$ l/min; **c** $\dot{V}_{O_2,SG} = 16$ l/min
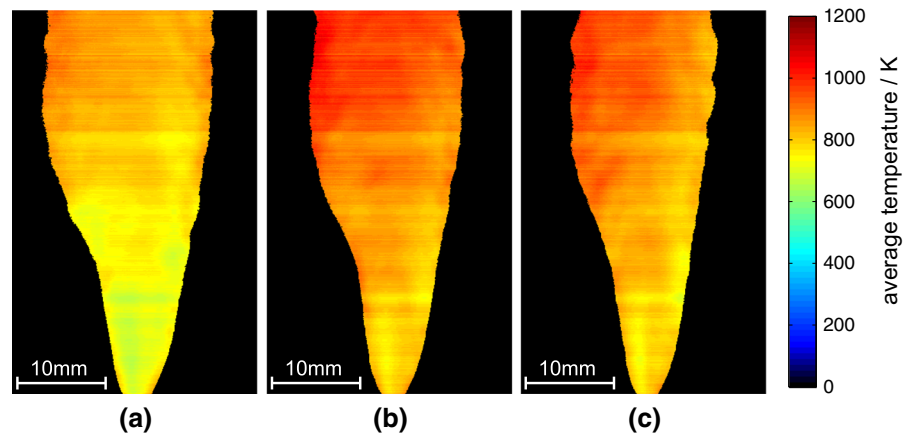
direction. For a 2D-fluence correction image, the integrated fluence curve is extracted and normalized. An exponential decay of the laser fluence through the flame is applied as an approximation with an absorption coefficient obtained from the extinction measurements. Finally, the correction image is weighted with the measured pulse energy of the OPO signal to obtain the relative fluence H. As the fluorescence signal is also partially absorbed within the flame respective to wavelength, a second correction has to be applied. With the approximation of a radially symmetric flame profile, the absorption length of the fluorescence signal is determined for each pixel, and the originally emitted fluorescence intensity is calculated assuming a roughly exponential signal decay. In a setup capable of simultaneous image acquisition for both wavelengths, the extinction measurements could be done in the same shot. These extinction corrections influence the resulting temperature by about 30 K. Applying the CARS calibration temperature and the spatially corresponding fluorescence signals (F_{32} and F_{31}) from TLAF measurements, C_t can be calculated according to the following equation:

$$C_t = \left(\frac{\Delta E_{21}}{T \cdot k_B} \right) + \ln\left(\frac{F_{31} \cdot H_{13}}{F_{32} \cdot H_{23}} \right) - 4\ln\left(\frac{\lambda_{32}}{\lambda_{31}} \right) \tag{2}$$

and results in $C_t = 2.96$. Therewith 2D-flame temperature distributions for different sheath gas flow rates ($\dot{V}_{O_2,SG}$) of 4.0, 10.0, 16.0 lmin^{-1} are calculated based on Eq. 1 using the laser fluence H instead of the irradiance I. Figure 4 shows the mean temperature distribution in the flame at different sheath gas flow

rates from 3 to 51.5 mm above the burner outlet. The flame structure in these images arises from the multiplication by a mask to exclude data with low signal-to-noise ratio. For the mask generation, fluorescence signal intensities smaller than a threshold value of 80 counts were zeroized in the average image for an excitation wavelength of 410.18 nm. As it can be seen in Fig. 4 for 4 lmin^{-1}, the mean temperature is about 90 K smaller in comparison to 10 lmin^{-1}. By raising the sheath gas flow rate to 16 lmin^{-1}, the measured mean temperature drops back down by 30 K.

Generally, the temperature in a FSP flame is substantially influenced by entrainment of ambient gas into the flame (Heine et al. 2006; Tricoli and Elmøe 2012). The ratio between the total gas mass flow $\dot{m}_t$ and the initial gas mass flow $\dot{m}_i$ through the nozzle may be described by (Han and Mungal 2001)

$$\frac{\dot{m}_t}{\dot{m}_i} = K_e \cdot \frac{\text{HAB}}{d}, \tag{3}$$

where K_e denotes the entrainment constant and d is the nozzle diameter. For a HAB = 40 mm and a nozzle diameter of 1.8 mm, Heine et al. calculated a ratio $\dot{m}_t/\dot{m}_i = 6.7$, corresponding to an entrainment constant of $K_e = 0.30$. Tricoli and Elmøe obtained an entrainment constant of $K_e = 0.23$ for 200 mm HAB and a total nozzle diameter of $d = 1.17$ mm. In either case, the entrainment constant K_e was obtained for relatively high positions in the flame, where K_e is expected to level off at a constant value. Following the approach of Tricoli and Elmøe, we performed the calculation at a position of 51 mm HAB for the FSP

flame with a sheath gas flow rate of 10 lmin^{-1}. An enthalpy feed rate of 177 kJmin^{-1} and a resulting total gas flow of 185 lmin^{-1}, corresponding to $\dot{m}_t = 240\,\text{gmin}^{-1}$, were obtained for 1007 K. For the initial mass flow of $\dot{m}_i = 11.1\,\text{gmin}^{-1}$ and a total nozzle diameter of 0.62 mm, an entrainment constant of $K_e = 0.26$ was obtained agreeing well with the literature. It should be noted that Tricoli and Elmøe in their calculations assume stoichiometric combustion, i.e., all educts are just fully converted. In order to explain the effects of varying sheath gas flows, which are much smaller than the total flow rates of entrained gas, on flame temperature, the following tentative explanation may be given. For a flow rate of 10 lmin,$^{-1}$ maximum temperatures are found, and it can be assumed that reaction conditions are close to stoichiometric. At 4 lmin,$^{-1}$ initial supply of oxygen through the sheath gas is not large enough to result in stoichiometric combustion, and thus, the initial slight fuel excess results in lower initial temperatures and overall in somewhat lower temperatures throughout the flame. Increasing the sheath gas to 16 lmin^{-1} increases the initial entrainment of oxygen in lower flame regions and thus slightly decreases the initial flame temperature due to the lean combustion. The lower initial temperature results in a decreased flame temperature even in higher flame regions as compared to 10 lmin^{-1}. Müller et al. (2004) and Mädler et al. (2002) measured temperatures in FSP flames (precursor: zirconium n-propoxide and hexamethyldisiloxane in ethanol, respectively) with a somewhat different geometry by FTIR E/T spectroscopy and partially found temperatures above 2000 K. In FTIR E/T, the mean flame temperature along a line-of-sight is obtained by fitting a blackbody Planck function through the hot CO_2 bands from 2300 to 2200 cm^{-1}. Compared to those temperatures, the mean temperatures measured in this study are substantially lower. A possible reason for this difference might be founded in the different operating principles of the two techniques. FTIR measures a temperature along a line-of-sight that is dominated by hot CO_2 bands. Colder regions, such as from the entrainment of ambient gas, are hardly accounted for, so it may be assumed that FTIR is biased toward higher temperatures. With TLAF, local temperatures are measured, with the present setup also temporally averaged, similar to FTIR. The calibration of the present TLAF

measurements relies on pure rotational CARS measurements (Engel et al. 2012). Generally, the CARS technique is regarded as a standard for highly accurate thermometry in flames (Roy et al. 2010). The CARS measurements in the FSP flame performed by Engel et al. (2012) reveal temperatures mostly significantly below 2000 K. At a point on the flame axis, they find a bimodal temperature distribution with peaks around 670 and 1794 K, respectively. This bimodal distribution is caused by the turbulent character of the flame where at various times either cold or hot zones, respectively, are present. With the temporal averaging in our setup, flame temperatures are expected to be in between these values as it is indeed the case. Comparing results from 2D-TLAF measurements of this study with the corresponding CARS measurements at nine positions for a sheath gas flow rate of 10 lmin,$^{-1}$ the root mean square deviation can be calculated as $\sigma_T = 67.5$ K. As shown in Fig. 4, this uncertainty may be largely due to imperfect laser sheet intensity corrections, which are not apparent in the raw images in Fig. 3 and only become apparent after laser sheet intensity normalization. This can be improved in future work by utilizing a simultaneous acquisition of individual laser sheet profiles for spatio-temporally resolved shot-to-shot corrections.

Conclusion

In the present paper, TLAF was successfully applied to an indium-based FSP process. The study verifies the capability and potential of this technique for two-dimensional temperature measurements during particle formation without additional indium seeding. It also showed that this approach can provide new insight into the physical mechanisms that affect the temperature distribution and, therefore, nanoparticle formation. These experimental temperature data are important for modeling and simulation of the particle formation mechanism and kinetics in the flame to improve the process and thereby the particle properties such as particle size, morphology, and crystallinity. As only a single OPO and detection system was available for both excitation wavelengths, no time-resolved temperature measurements were possible. The results, however, demonstrate that the technique holds the possibility for single-shot temperature measurements in a turbulent indium-based FSP flame with the

availability of two OPO systems. Based on signal-to-noise ratios obtained so far, a precision of 11 K may be estimated.

References

Arabi-Katbi OI, Pratsinis SE, Morrison PW Jr, Megaridis CM (2001) Monitoring the flame synthesis of TiO_2 particles by in-situ FTIR spectroscopy and thermophoretic sampling. Combust Flame 124:560–572

Bessler WG, Hildenbrand F, Schulz C (2001) Two-line laser-induced fluorescence imaging of vibrational temperatures in a NO-seeded flame. Appl Opt 40:748–756

Bohlin A, Kliewer CJ (2013) Communication: two-dimensional gas-phase coherent anti-Stokes Raman spectroscopy (2D-CARS): simultaneous planar imaging and multiplex spectroscopy in a single laser shot. J Chem Phys 138:221101

Camenzind A, Strobel R, Pratsinis SE (2005) Cubic or monoclinic Y2O3:Eu3+ nanoparticles by one step flame spray pyrolysis. Chem Phys Lett 415:193–197

Daily JW (1997) Laser induced fluorescence spectroscopy in flames. Prog Energy Combust Sci 23:133–199

Dec JE, Keller JO (1986) High speed thermometry using two-line atomic fluorescence. Symp (Int) Combust 21:1737–1745

Engel SR, Koegler AF, Gao Y, Kilian D, Voigt M, Seeger T, Peukert W, Leipertz A (2012) Gas phase temperature measurements in the liquid and particle regime of a flame spray pyrolysis process using O2-based pure rotational coherent anti-Stokes Raman scattering. Appl Opt 51:6063–6075

Fix A, Haub JG, Johnson MJ, Schröer T, Wallenstein R, Orr BJ (1993) Tunable beta-barium borate optical parametric oscillator: operating characteristics with and without injection seeding. J Opt Soc Am B 10:1744–1750

Gopchandran KG, Joseph B, Abraham JT, Koshy P, Vaidyan VK (1997) The preparation of transparent electrically conducting indium oxide films by reactive vacuum evaporation. Vacuum 48:547–550

Han D, Mungal MG (2001) Direct measurement of entrainment in reacting/nonreacting turbulent jets. Combust Flame 124:370–386

Hartlieb AT, Atakan B, Kohse-Höinghaus K (2000) Temperature measurement in fuel-rich non-sooting low-pressure hydrocarbon flames. Appl Phys B 70:435–445

Haudiquert M, Cessou A, Stepowski D, Coppalle A (1997) OH and soot concentration measurements in a high-temperature laminar diffusion flame. Combust Flame 111:338–349

Heine MC, Mädler L, Jossen R, Pratsinis SE (2006) Direct measurement of entrainment during nanoparticle synthesis in spray flames. Combust Flame 144:809–820

Hult J, Burns IS, Kaminski CF (2005) Two-line atomic fluorescence flame thermometry using diode lasers. Proc Combust Inst 30:1535–1543

Jang HD, Seong CM, Chang HK, Kim HC (2006) Synthesis and characterization of indium-tin oxide (ITO) nanoparticles. Curr Appl Phys 6:1044–1047

Joklik RG, Horvath JJ, Semerjian HG (1991) Temperature measurements in flames using thermally assisted laser-induced fluorescence of Ga. Appl Opt 30:1497–1504

Kammler HK, Jossen R, Morrison PW Jr, Pratsinis SE, Beaucage G (2003) The effect of external electric fields during flame synthesis of titania. Powder Technol 135–136:310–320

Kammler HK, Mädler L, Pratsinis SE (2001) Flame synthesis of nanoparticles. Chem Eng Technol 24:583–596

Kilian D, Engel S, Borsdorf B, Gao Y, Kögler AF, Kobler S, Seeger T, Will S, Leipertz A, Peukert W (2014) Spatially resolved flame zone classification of a flame spray nanoparticle synthesis process by combining different optical techniques. J Aerosol Sci 69:82–97

Kohse-Höinghaus K (1994) Laser techniques for the quantitative detection of reactive intermediates in combustion systems. Prog Energy Combust Sci 20:203–279

Kronemayer H, Ifeacho P, Hecht C, Dreier T, Wiggers H, Schulz C (2007) Gas-temperature imaging in a low-pressure flame reactor for nano-particle synthesis with multi-line NO-LIF thermometry. Appl Phys B 88:373–377

Liu X, Smith ME, Tse SD (2010) In situ Raman characterization of nanoparticle aerosols during flame synthesis. Appl Phys B 100:643–653

Mädler L, Kammler HK, Mueller R, Pratsinis SE (2002) Controlled synthesis of nanostructured particles by flame spray pyrolysis. J Aerosol Sci 33:369–389

Medwell PR, Chan QN, Kalt PAM, Alwahabi ZT, Dally BB, Nathan GJ (2009) Development of temperature imaging using two-line atomic fluorescence. Appl Opt 48:1237–1248

Miller JD, Engel SR, Meyer TR, Seeger T, Leipertz A (2011) High-speed CH planar laser-induced fluorescence imaging using a multimode-pumped optical parametric oscillator. Opt Lett 36:3927–3929

Miller JD, Engel SR, Tröger JW, Meyer TR, Seeger T, Leipertz A (2012) Characterization of a CH planar laser-induced fluorescence imaging system using a kHz-rate multimode-pumped optical parametric oscillator. Appl Opt 51:2589–2600

Müller D, Pagel R, Burkert A, Wagner V, Paa W (2014) Two-dimensional temperature measurements in particle loaded technical flames by filtered Rayleigh scattering. Appl Opt 53:1750–1758

Müller R, Jossen R, Kammler HK, Pratsinis SE, Akhtar MK (2004) Growth of zirconia particles made by flame spray pyrolysis. AIChE J 50:3085–3094

Murali A, Barve A, Leppert VJ, Risbud SH, Kennedy IM, Lee HWH (2001) Synthesis and characterization of indium oxide nanoparticles. Nano Lett 1:287–289

Nygren J, Engström J, Walewski J, Kaminski CF, Aldén M (2001) Applications and evaluation of two-line atomic LIF

thermometry in sooting combustion environments. Meas Sci Technol 12:1294

Rasbach U, Wang J, dela Torre R, Leung V, Klöter B, Meschede D, Varzhapetyan T, Sarkisyan D (2004) One- and two-color laser spectroscopy of indium vapor in an all-sapphire cell. Phys Rev A 70:033810

Roy S, Gord JR, Patnaik AK (2010) Recent advances in coherent anti-Stokes Raman scattering spectroscopy: fundamental developments and applications in reacting flows. Prog Energy Combust Sci 36:280–306

Solomon PR, Best PE (1991) Fourier transform infrared emission/transmission spectroscopy in flames. In: Chigier N (ed) Combustion measurements, vol 1. Hemisphere Publishing Corporation, New York, pp 385–444

Stricker WP (2002) Measurement of temperature in laboratory flames and particle devices. In: Kohse-Höinghaus K, Jeffries JB (eds) Combustion applied diagnostics. Taylor and Francis, New York, pp 155–193

Strobel R, Pratsinis SE (2007) Flame aerosol synthesis of smart nanostructured materials. J Mater Chem 17:4743–4756

Teoh WY, Amal R, Madler L (2010) Flame spray pyrolysis: an enabling technology for nanoparticles design and fabrication. Nanoscale 2:1324–1347

Tricoli A, Elmøe TD (2012) Flame spray pyrolysis synthesis and aerosol deposition of nanoparticle films. AIChE J 58:3578–3588